



**ZrO₂ Atomic Layer Deposition Into Sr_{0.5}Sm_{0.5}CoO_{3-δ}-
Ce_{0.9}Gd_{0.1}O_{2-δ} Solid Oxide Fuel Cell Cathodes: Mechanisms
of Stability Enhancement**

Journal:	<i>Journal of Materials Chemistry A</i>
Manuscript ID	TA-ART-08-2019-009214.R1
Article Type:	Paper
Date Submitted by the Author:	06-Nov-2019
Complete List of Authors:	Schmauss, Travis; Northwestern University, Materials Science and Engineering Railsback, Justin; Northwestern University, Materials Science and Engineering Lu, Matthew; Northwestern University, Materials Science and Engineering Zhao, Kevin; Northwestern University, Materials Science and Engineering Barnett, Scott; Northwestern University, Materials Science and Engineering

ZrO₂ Atomic Layer Deposition Into Sr_{0.5}Sm_{0.5}CoO_{3-δ}-Ce_{0.9}Gd_{0.1}O_{2-δ} Solid Oxide Fuel Cell Cathodes: Mechanisms of Stability Enhancement

Travis A. Schmauss^a, Justin G. Railsback^a, Matthew Y. Lu^a, Kevin Y. Zhao^a, Scott A. Barnett^{a*}

^aDepartment of Materials Science and Engineering, Northwestern University, Evanston, IL 60208. E-mail: s-barnett@northwestern.edu

Abstract: The application of atomic layer deposition (ALD) on solid oxide fuel cell (SOFC) cathodes has previously yielded mixed results and has been seen to depend on the ALD species, catalyst chemistry, catalyst morphology, and the conditions for deposition. Characterized here is the effect of an ALD zirconia coating within an SOFC oxygen electrode: Sr_{0.5}Sm_{0.5}CoO_{3-δ} infiltrated into Gd-doped ceria, Ce_{0.9}Gd_{0.1}O_{2-δ}, scaffolds (SSC-GDC). Island-like ALD-ZrO₂ coatings with approximately monolayer coverage initially yield a higher electrode polarization resistance, R_p, but thereafter the coated electrodes show lower R_p and slower degradation. For example, after ~1000 hour accelerated ageing tests carried out at 750°C, SSC-GDC coated with ~0.3 nm of ALD-ZrO₂ showed an R_p increase of 18% compared to 30% for uncoated SSC-GDC. Strontium surface segregation was not found to be a significant degradation factor. At 750°C, a reaction between the Zr-overlayer and the SSC was observed, producing SrZrO₃, Co₃O₄, and SmCoO₃. The low R_p values achieved suggest that the reactant products were thin enough to be discontinuous and thus not hinder the oxygen surface exchange process, and yet they acted as a barrier to SSC particle coarsening.

I. Introduction

Low temperature (400-650°C) solid oxide fuel cells (SOFCs) are being developed to improve system economics, *e.g.* via lowering balance-of-plant costs and extending SOFC stack lifetimes.¹ However, low-temperature oxygen electrodes typically utilize highly active, nano-scale mixed ionic-electronic conductors (MIECs) such as Sr_{0.5}Sm_{0.5}CoO_{3-δ} (SSC)² to accelerate the sluggish oxygen reduction reaction. These electrodes are susceptible to degradation phenomena such as microstructural coarsening that are exacerbated by decreasing electrode feature sizes, but are fabricated as such in an attempt to reduce low-temperature polarization resistance, R_p.²⁻⁵ Recent studies suggest that the need to maintain long-term stability by reducing coarsening will limit the R_p that can be achieved at low temperatures.^{5,6}

Atomic layer deposition (ALD) of thin, conformal ZrO₂ has recently been applied to SOFC cathodes with the aim of limiting degradation.⁷ ZrO₂ overlayers were shown to curb degradation of infiltrated La_{0.6}Sr_{0.4}CoO_{3-δ} (LSC) in La_{0.80}Sr_{0.20}Ga_{0.83}Mg_{0.17}O_{3-δ} (LSGM) scaffolds⁸ and La_{0.6}Sr_{0.4}Fe_{0.8}Co_{0.2}O_{3-δ} (LSCF)/GDC composite scaffolds.⁹ It has been suggested that the applied ALD layers are porous and may exhibit mixed conductivity due to diffusion of impurities (*e.g.*, Fe

or Co) from the MIEC into the ZrO_2 lattice, such that the resultant doped zirconia allows for the reduction of O_2 . Two mechanisms for the ALD stability improvement have been suggested – suppression of MIEC coarsening and/or inhibition of cation surface segregation. Coarsening could be mitigated if the ALD layer acted as a barrier to the underlying catalytic layer's self-diffusion, whereas it is posited that cation segregation could be mitigated via formation of a negative space charge region⁸ or a decrease in the number of positive electron holes.⁹ However, other cases of ALD- ZrO_2 applied to both an infiltrated and composite system, *e.g.* $\text{La}_{0.8}\text{Sr}_{0.2}\text{FeO}_{3-\delta}$ -yttria-stabilized zirconia scaffold (LSF-YSZ)¹⁰ and LSCF/GDC,¹¹ were found to have provided no benefit to performance and were suggested to have irreversibly blocked active sites. In this case, deposition conditions differed: rather than purging excess reactant/reaction products by continuously flowing carrier gas, vacuum was pulled after each pulse of precursor for their removal.

Results using ALD oxides other than ZrO_2 on SOFC cathodes have been mixed as well. ALD- CoO_x on LSC thin films led to increased polarization resistance,¹² but lower resistance was successfully achieved on a $\text{La}_{0.8}\text{Sr}_{0.2}\text{MnO}_{3-\delta}$ (LSM)/YSZ composite scaffold.¹³ Additionally, ALD- Al_2O_3 on $\text{La}_{0.8}\text{Sr}_{0.2}\text{FeO}_{3-\delta}$ (LSF) infiltrated into YSZ,¹⁴ and CeO_x and SrO on LSF, LSC, and $\text{Ba}_{0.5}\text{Sr}_{0.5}\text{Co}_{0.8}\text{Fe}_{0.2}\text{O}_3$ (BSCF) infiltrated into YSZ,¹⁵ were all found to hinder cell performance, while Bi_2O_3 on LSM scaffolds,¹¹ LaO_x on LSF/YSZ,¹⁰ and a $\text{LaO}_x/\text{SrO}_x/\text{CoO}_x$ super-cycle onto a LSCF thin film¹⁶ increased performance. Factors of precursor, the underlying catalytic substrate, and the deposition parameters used may all be important in combination for determining the performance of an ALD-modified electrode.

In this study, we analyze the effect of the most commonly applied ALD species, ZrO_2 , on the electrochemical properties and stability of cathodes made by infiltrating SSC into GDC scaffolds (SSC-GDC) on a GDC electrolyte. This system was previously studied in detail to model degradative effects, thought mainly to be caused by coarsening;³ the present results extend the life-testing to ALD- ZrO_2 -coated SSC-GDC electrodes. Furthermore, extensive characterization was carried out to determine the actual ALD layer thickness in the electrode active region and the reactions between the ALD layer and the SSC. The results indicate that with careful control of the ALD- ZrO_2 thickness, electrode stability can be improved due to the presence of a very small amount of zirconate phase in the MIEC active layer.

II. Experimental

Cell fabrication – Cells were processed using the procedure described in detail elsewhere.³ Briefly, identical $\text{Ce}_{0.9}\text{Gd}_{0.1}\text{O}_{2-\delta}$ (GDC) (Rhodia) layers were screen printed on opposite sides of dense GDC electrolyte pellets and fired at 1100°C for 4 h, yielding porous scaffolds with $\sim 20\ \mu\text{m}$ thickness and an area of $\sim 0.5\ \text{cm}^2$. A nitrate solution was then infiltrated into the porous GDC layers and calcined at 800°C for 0.5 h; this procedure was repeated ~ 8 times to yield

stoichiometric SSC nanoparticles decorating the GDC pore surfaces with a volume fraction of ~20%. $\text{La}_{0.8}\text{Sr}_{0.2}\text{MnO}_{3-\delta}$ (LSM) was screen printed over the infiltrated scaffolds and fired at 800°C for 2 h to yield porous current collector layers ~10 μm thick. Cells used for imaging and for generating Fig. S1 were identical except for ~35 μm SSC-GDC layers and ~20 μm LSM. For electrochemical testing, silver grids and wires were then affixed to the electrodes. SEM (Hitachi SU-8030) and EDS (Oxford AZtec X-max 80 SDD) maps of the porous scaffold layers were generated for fracture cross-sections, which were plasma-coated in osmium for conductivity.

SSC powder characterization – SSC nanopowder with <50 nm particle size and >25 m^2/g specific surface area (MilliporeSigma) was used as an analog for the SSC electrodes, allowing additional characterization of the interaction of ALD- ZrO_2 with SSC. Microscopy was done using a Hitachi HD-2300 scanning transmission electron microscope (STEM) in brightfield mode using SSC powder suspended in ethanol, sonicated, and pipetted onto lacey carbon grids. X-ray powder diffraction was carried out using a STOE Stadi-P with $\text{Cu K}\alpha$ radiation. Inductively coupled plasma-optical emission spectroscopy (ICP-OES, Thermo iCAP 7600) was used for quantification of water-soluble Sr species. For this, the SSC powder was prepared by agitating in a vortex mixer for 5 minutes in a solution of MilliPore water and filtered through Amicon Ultra-4 Centrifugal Filter Units. The powder composition was checked by ICP-OES, after dissolving in 1:1 hydrochloric and nitric acid, and was found to be $\text{Sr}_{0.47\pm 0.01}\text{Sm}_{0.42\pm 0.01}\text{Co}_{1\pm 0.12}\text{O}_x$.

ZrO_2 atomic layer deposition – ALD was carried out using either a Savannah S100 or Arradiance GEMstar-8 ALD system. The ALD cycle consisted in sequence of: (1) 0.15s pulse of $\text{H}_2\text{O}_{(\text{v})}$; (2) 5s N_2 gas purge; (3) 0.40s pulse Tetrakis(dimethylamino)zirconium(IV) (TDMAZ); and (4) 5s N_2 gas purge. Three sample configurations were coated. SSC powder was coated with 7 cycles by dispersing in ethanol, pipetting onto glass or silicon, and then drying. For STEM studies, SSC powder on TEM grids was coated using 3, 30, and 60 cycles by enclosing the grids in a vented Al-foil cage inside the ALD chamber. SSC-GDC electrodes in symmetric cells were coated with 30, 60, and 300 cycles; deposition on both electrodes was allowed by suspending the cells over the substrate holder using glass slides or clips at the edges of the cells. The ZrO_2 thickness decreases significantly with increasing depth into the electrodes, and this effect is quantified below. A similar effect presumably also occurs in coating SSC powders, such that ALD coating effects observed in powders are probably reduced due to a lesser ZrO_2 thickness.

Electrochemical characterization and life-testing – All testing was done in air using electrochemical impedance spectroscopy (EIS, Zahner IM6) in the frequency range of $10^6 - 10^{-1}$ Hz. The cells were first ramped to 600°C for an initial EIS measurement and then ramped to the accelerated ageing temperature of 750°C where they remained except for periodic decreases to 600°C for EIS measurements. The cycle of ramping down, testing, and ramping up took ~2 hours

and <4% of the total ageing time. A schematic of a similar life-test schedule is given elsewhere.³ The SSC-GDC cells were fabricated in the same batch using identical materials and conditions in order to facilitate meaningful comparisons. The dataset for the uncoated SSC-GDC electrode (*i.e.*, with no ALD coating) was first published by Call *et al.*³ The commercial SSC particles were aged in air at 750°C. The impedance data fitting was performed using a software¹⁷ programmed in Python which relies on the scientific Python stack.^{18–20}

III. Results

The effects of ALD-ZrO₂ on electrode electrochemical characteristics and scaffold chemistry and morphology are described in Section A. The characteristics of the ALD process, particularly the ZrO₂ thickness distribution versus position in the electrode, are described in Section B. Further characterization probing the effects of ALD-ZrO₂ and its interactions with SSC, using SSC nanopowder as a surrogate for the SSC-infiltrated electrode, is detailed in Section C.

A. Electrochemical characterization

The EIS data of the coated and uncoated cells are summarized in Fig. 1, with the high-frequency intercept impedance, Z' , set to 0 for all cells to highlight changes in the polarization response. The total polarization resistance values, R_p , measured within 1 h of reaching 600°C, are higher for the ZrO₂-coated cells than for the uncoated cell. However, after ageing for 48 hours at 750°C and returning to 600°C for testing, the coated electrode R_p values have dropped below that of the uncoated electrode, suggesting that the 750°C treatment yields considerable changes in the ZrO₂-coated SSC-GDC cells. A small decrease in polarization resistance for the uncoated electrode is also seen, which has been described previously as a break-in effect.^{21,22}

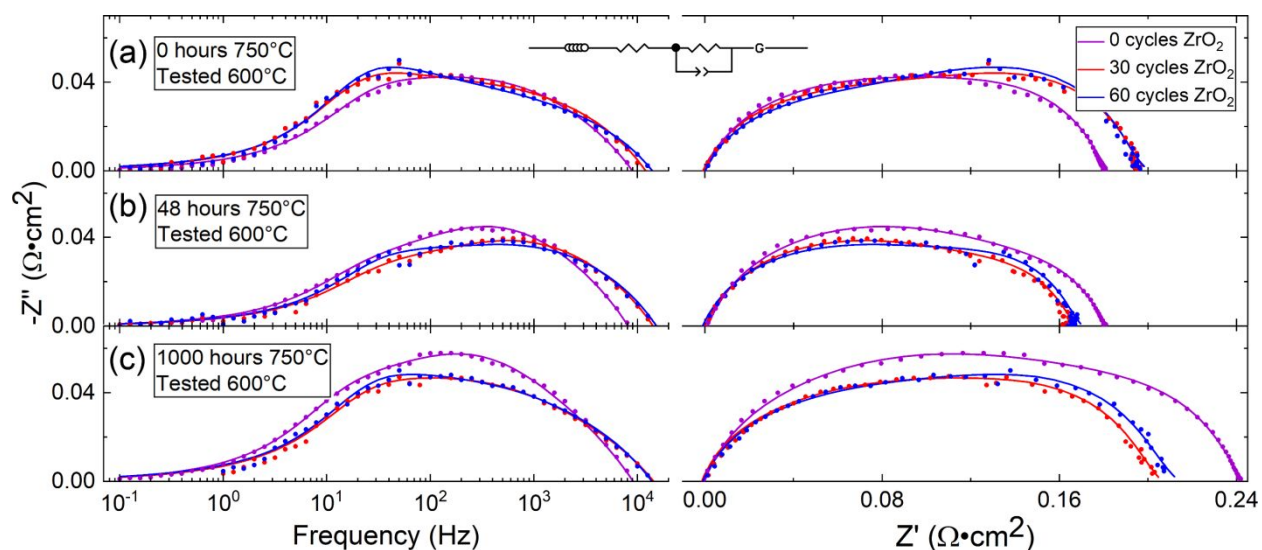


Fig. 1. Bode and Nyquist plots of EIS spectra taken at 600°C from 0, 30, and 60 cycles ALD-ZrO₂-coated SSC-GDC cells, taken at 600°C (a) shortly after the initial heating of the cell to 600°C, (b) after approximately 48 hours of ageing at 750°C, and (c) after approximately 1000 hours of ageing at 750°C. Data is fit with an equivalent circuit consisting of an inductor, resistor, high frequency RQ element, and low frequency Gerischer element in series.³

The spectra were fit well by an equivalent circuit consisting of an inductor associated with the measurement circuit wiring, a resistor representing electrolyte ohmic resistance, a high frequency RQ element usually associated with solid-solid interfaces, and a low frequency Gerischer element accounting for electrochemical reaction and oxygen transport processes in the electrode, all in series.³ R_p values, taken as the sum of the RQ and Gerischer resistances, were logged periodically throughout the life test and are displayed in Fig. 2. After an initial decrease, R_p values steadily increase during the tests. However, the time rates of R_p increase for the ZrO₂-coated electrodes are less than for the uncoated electrode. These trends were reproduced in a second set of life tests aged at 800°C, with the best overall performance again achieved by the 30-cycle ALD-ZrO₂ coating cell (Supplementary Fig. S1). In summary, the electrochemical results show a small but clearly measurable improvement in stability for the ALD-modified electrodes.

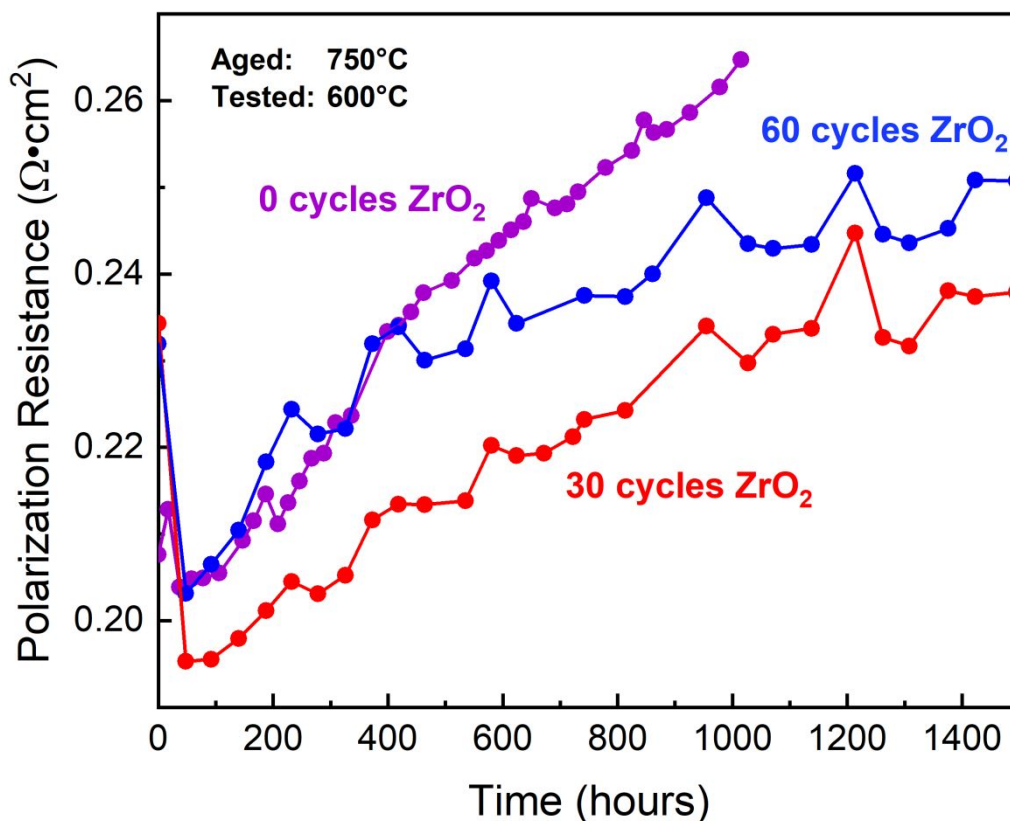


Fig. 2. Time dependence of the polarization resistance measured in air at 600°C for cells with 0, 30, and 60 cycle ALD-ZrO₂ coated SSC-GDC electrodes. Cells were maintained at an accelerated ageing temperature of 750°C except during periodic interruptions for EIS measurements.

B. ALD Zirconia Layer Characterization

It is well known that ALD coating thickness can decrease with increasing depth into a porous structure, depending on the ALD cycle conditions.^{23,24} This results when the distance that a precursor molecule has to traverse before adsorbing onto unreacted surface, relative to the pore size, is large, and subject to slow Knudsen-limited diffusion. Depending on the ALD precursor, this diffusion distance can be overcome with long soak times, but for less stable precursors, each collision with inner pore surfaces subjects the precursor to a possibility of CVD-like thermal decomposition.^{25,26} Furthermore, it is difficult to directly measure the ALD thickness versus depth within the porous electrode given the discrepancy in length scales between coating and scaffold. Thus, an indirect method was used to estimate ALD zirconia thickness versus depth in the electrode: the nominal zirconia thickness at the electrode free surface was scaled using the measured Zr content versus position.

The ALD coating thickness was characterized by depositing onto ~16 nm SSC powder; this provided a surrogate that was similar to the infiltrated SSC electrode of ~50 nm starting particle size,³ but with two advantages. First, depth of penetration effects were minimized for the thin, loosely-packed powder bed compared to the electrode, providing a thickness representative of the electrode free surface. Second, the powder could be prepared for STEM imaging with minimal processing, and hence minimal artifacts. Fig. 3 (a) and (b) show the morphology of uncoated powder and after 3 ALD cycles, respectively. The 3-cycle case shows a discontinuous coating of ~3 nm diameter ZrO₂ islands on the surface of the SSC, so it is difficult to estimate the nominal thickness. Such island formation has been reported in very thin ALD layers.^{27,28} Using the same Zr precursor and deposition temperature as in the present case, a uniformly thick layer was not observed until 40 cycles.²⁹ Also shown are typical images from (c) 30 and (d) 60 cycles of growth with uniformly thick, dense ZrO₂ layers. Layer thicknesses were measured to be 4.5 ± 0.8 nm for 30 cycles (averaged over 38 particles) and 7.5 ± 0.9 nm after 60 cycles (averaged over 58 particles) which correspond to growth-per-cycle (GPC) values of 0.15 ± 0.03 nm/cycle and 0.13 ± 0.01 nm/cycle. The 60-cycle GPC of 0.13 nm/cycle is less than a report of a similar process on perovskite nanoparticles (0.167 nm/cycle)⁸ but higher than reported for a flat silicon substrate after many cycles (0.096 nm/cycle).³⁰

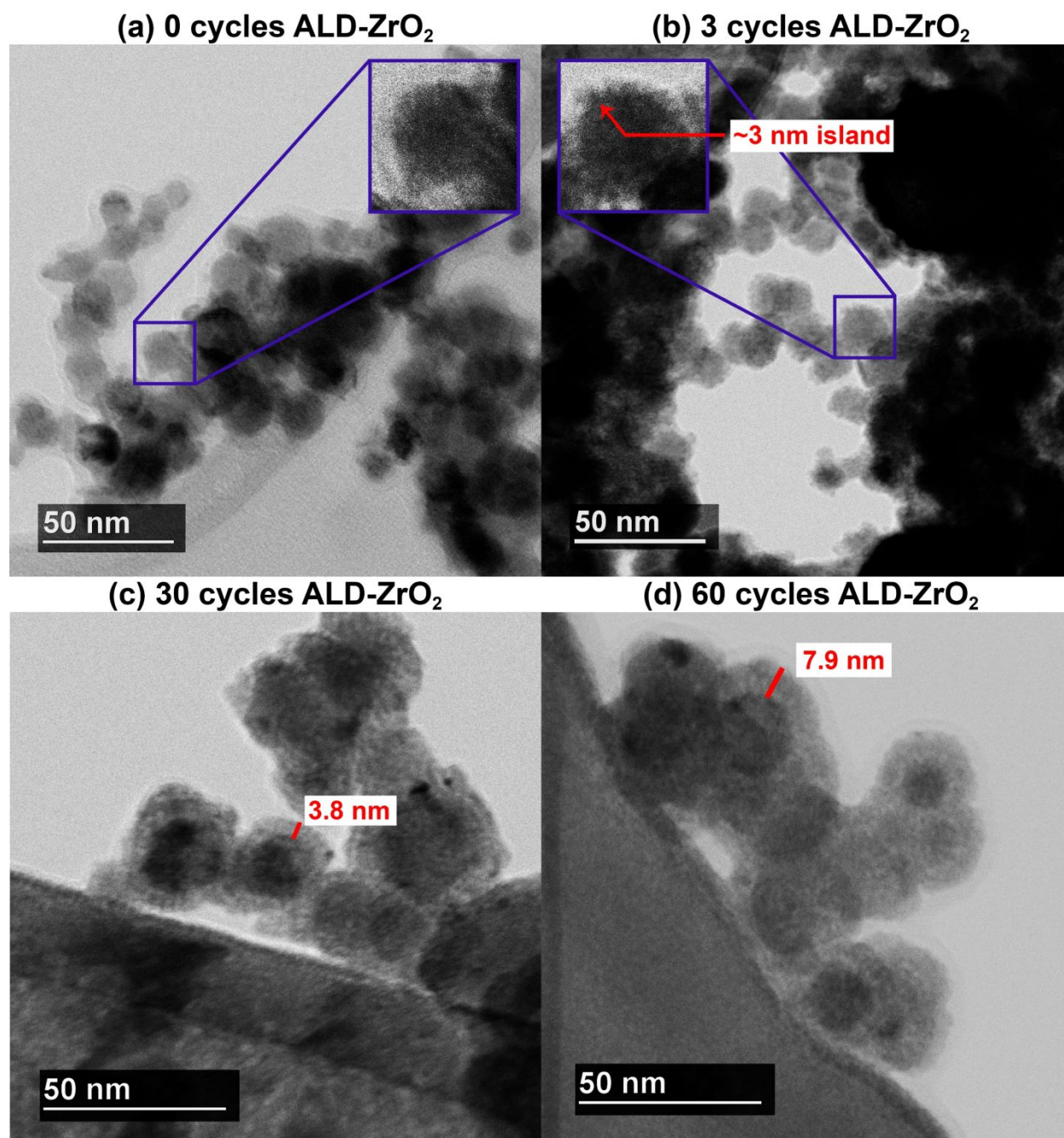


Fig. 3. STEM images of SSC powders, with (a) 0, (b) 3, (c) 30, and (d) 60 cycles of ALD-ZrO₂ with superimposed measures of representative coating thicknesses. Sub-monolayer growth is visible in (b) transitioning to a layer-by-layer growth-per-cycle at higher cycle numbers.

Fig. 4 (a) shows a fracture cross-sectional SEM image of the electrode region used for compositional mapping, including an $\sim 20 \mu\text{m}$ porous LSM current collector, an $\sim 40 \mu\text{m}$ thick SSC-GDC layer, and a portion of the GDC electrolyte. The microstructure is similar to that reported previously.³ This electrode had been coated with an unusually high number of ALD-ZrO₂ cycles,

300, to improve the Zr EDS signal. The SEM-EDS compositional depth profile (Fig. 4 (b)) shows the EDS signal intensities of Zr and other key elements versus depth perpendicular to the cell layers, generated by averaging intensities across the region shown in (a). The Co, Ce, and La signals provide clear indications of where SSC, GDC, and LSM are present, respectively. The Zr signal is highest in the outer LSM layer, falling off rapidly within the first $\sim 20 \mu\text{m}$ of the SSC-GDC layer and approaching a minimum deeper into the electrode. The rise in intensity once the GDC electrolyte is reached is attributed to the higher EDS background from dense surfaces.

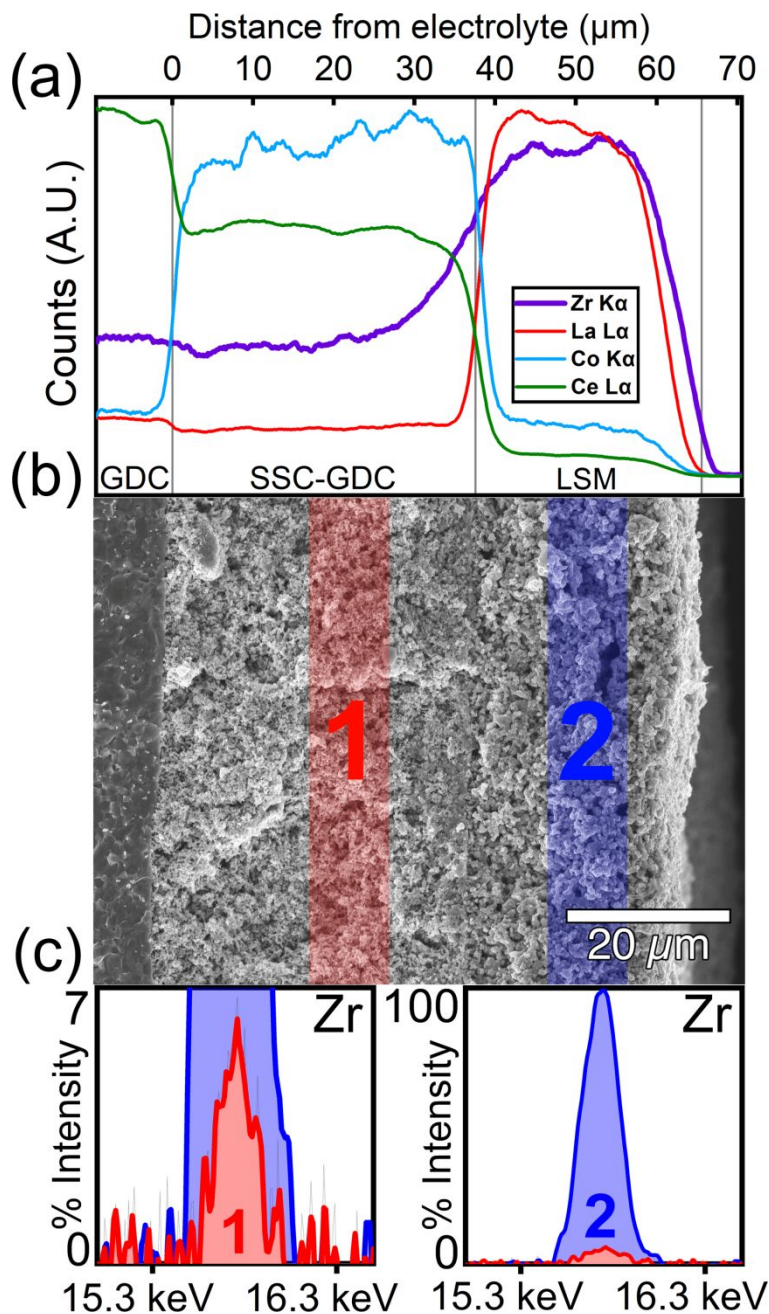


Fig. 4. (a) EDS line-scans of an SSC-GDC cathode coated with 300 cycles of ALD-ZrO₂. The Zr K α signal is significant near the surface, within the microstructurally less complex LSM current collector, and rapidly diminishes over a \sim 20 μ m depth as LSM transitions into the narrower pores of SSC-GDC. (b) An SEM micrograph of the three-layer region from which the line-scans in (a) were collected. (c) A comparison of the Zr K α peaks taken in the near-surface (LSM) region and within the active region of the tested electrode (labeled “2” and “1” in (b), respectively).

The decrease in EDS intensity with increasing depth suggests a decrease in ZrO₂ layer thickness. In order to quantify this, EDS spectra were compared in the near surface region (labeled “2” in Fig. 4 (b)) and a region within the SSC-GDC corresponding to the active region of the 20 μ m thick tested electrodes (labeled “1”). To obtain accurate values, the integrated intensities of the Zr EDS peaks in Fig. 4(c) were used, and a ratio of the intensities calculated. The thickness in region 1 was estimated to be \sim 7% the thickness of region 2. Thus, the average ZrO₂ thickness in the active region of the tested cells was \sim 0.3 nm for 30 cycles and \sim 0.5 nm for 60 cycles.

C. SSC-ZrO₂ Stability

In order to assess the role of Sr surface segregation in SSC, ICP measurements were carried out. Separate SSC powder samples were annealed at 750°C for varying times and the amount of surface strontium was measured. Sr-containing species including SrO, SrCO₃, and/or Sr(OH)₂ dissolve in ultrapure water that can be analyzed to determine the amount of segregated Sr.^{31,32} As shown in Fig. 5, the Sr amount was highest in the pristine state, dropped by a factor of 2 after a 10 h anneal, and then remained approximately constant at longer times. Note that the high initial Sr content was likely associated with the SrCO₃ phase present in this powder (see the XRD data below), which may actually be under-estimated due to the solubility limit of 11 ppm in water.³³ In any case, there is no evidence of an increase in Sr segregation with time, as observed for other perovskite electrodes such as LSCF.³¹

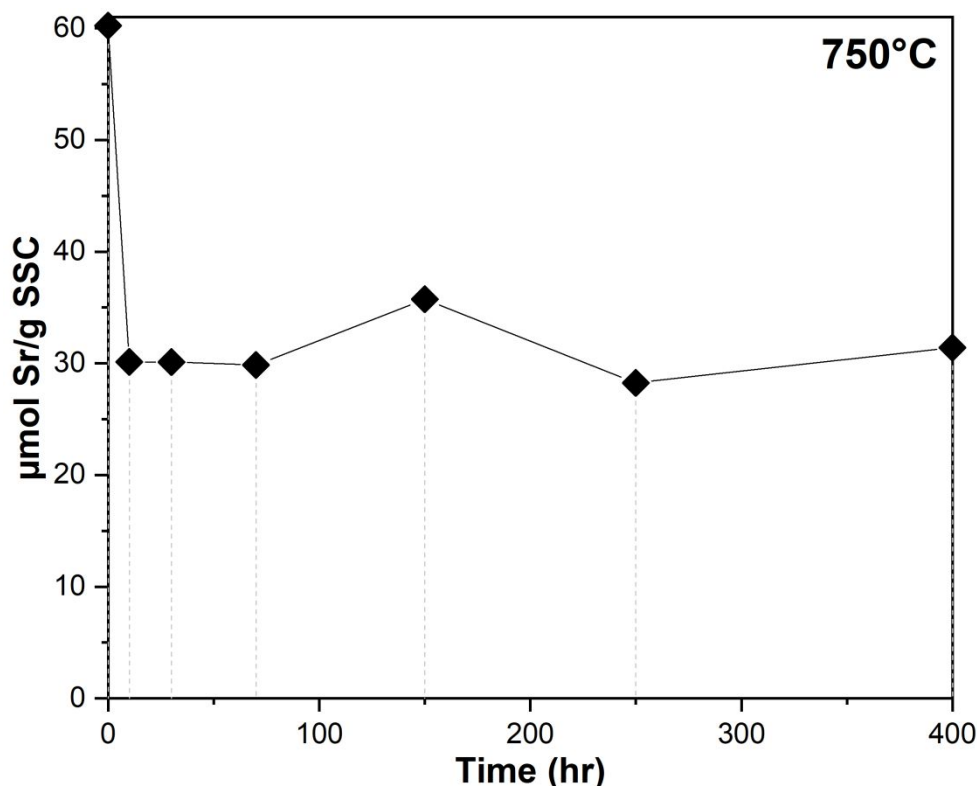
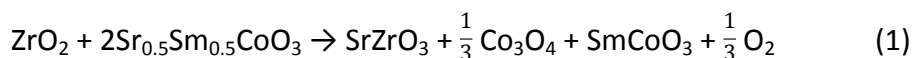


Fig. 5. Water-soluble surface strontium in SSC powder annealed for varying times at 750°C. The ionic amount of Sr is normalized by the mass of SSC used for measurement. At annealing times 10 hours and beyond, the Sr concentration does not evolve over time, indicating relative robustness of SSC against cation surface migration.

XRD scans of SSC powder and ALD-coated SSC powder before and after annealing are displayed in Fig. 6. The uncoated powder (a) shows a major SSC and minor SrCO₃ phase (the latter is eliminated upon heating to 750°C in air for 10 h, converting to surface SrO or incorporating into the SSC). Upon coating with 7 cycles of ALD-ZrO₂, (b), the XRD pattern looks almost identical to the uncoated powder; the lack of ZrO₂ diffraction is likely due to low ZrO₂ crystallinity. After annealing the coated powder for 10 hours at 750°C (c), the same SSC peaks remain, the SrCO₃ peak is eliminated, and SrZrO₃, Co₃O₄, and SmCoO₃ peaks appear. Crystalline zirconia phases are again not detected, presumably because all zirconia has been reacted. Formation of SrZrO₃ due to the reaction between many common Sr-containing perovskite electrodes and zirconia has been widely reported^{34–37} with the other two species likely arising by consequence of the resulting change in perovskite stoichiometry. Thus, a portion of the SSC, determined by the amount of ZrO₂ available is decomposed according to the reaction:



In the pattern shown in Fig. 6 (c), the amount of zirconia was small relative to the amount of SSC, such that SSC remains the predominant phase and the products are minority phases. In a case where a thicker ALD-ZrO₂ coating was applied to SSC powder and annealed at a higher temperature of 800°C, a Sm-zirconate was formed instead of SmCoO₃ and the SSC peak was significantly reduced (Fig. S2). The reactivity between the ALD-ZrO₂ and SSC may be heightened by the intimate contact between overlayer and substrate, and/or by the amorphous nature of the ZrO₂ – in contrast, in an experiment where SSC and YSZ powders were mixed and heated, no XRD evidence of SrZrO₃ formation was found until 900°C and SmZrO₃ was not observed up to 1000°C.³⁸

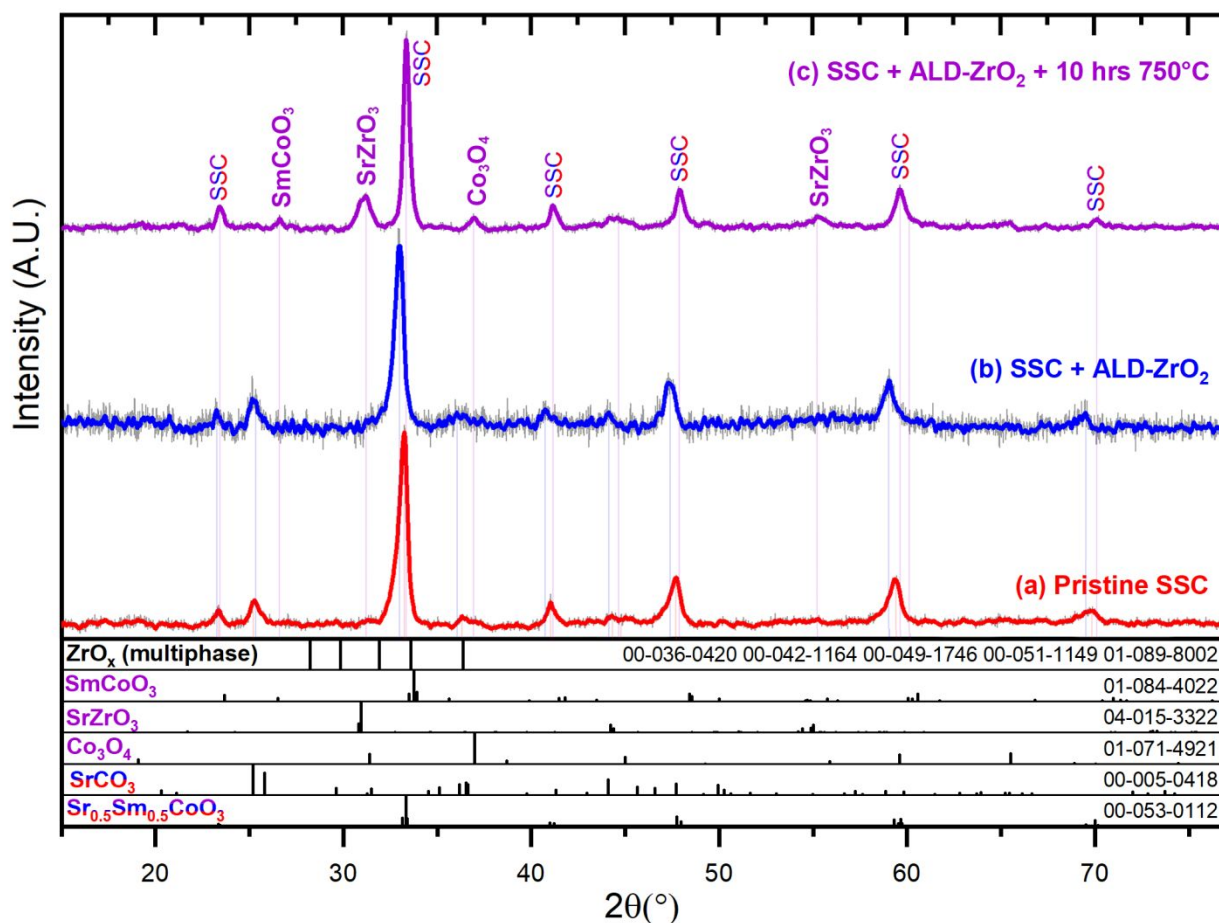


Fig. 6. XRD spectra of (a) pristine SSC powder with an SrCO₃ impurity, (b) SSC powder with ALD-ZrO₂ and without annealing, (c) ALD-ZrO₂-coated SSC after 10 hours of annealing at 750°C. Reference phase data and PDF card numbers are included in the 6 bottom panels for comparison, with zirconia being represented by the maximum intensity peaks from five major crystal systems.

Similar XRD scans of pristine SSC, annealed SSC, and annealed ALD-coated SSC are superimposed for comparison in Fig. 7. Of the three, the uncoated SSC powder shows the broadest peaks; an ALD-coated but not annealed SSC powder yielded a nearly identical shape to the uncoated SSC and is not shown for clarity. After annealing for 10 hours at 750°C, both coated and uncoated SSC peak widths were substantially reduced, but the uncoated SSC peak was narrower. Since a smaller full-width at half-maximum indicates a larger average crystallite size, it appears that there was substantial coarsening at the annealing conditions used, and that the presence of ALD-ZrO₂ influenced the resultant crystallite size. Using the Scherrer equation,³⁹ the estimated initial SSC crystallite diameter of 16.3 nm increases after annealing to 35.6 nm without the coating and 34.3 nm with the coating.

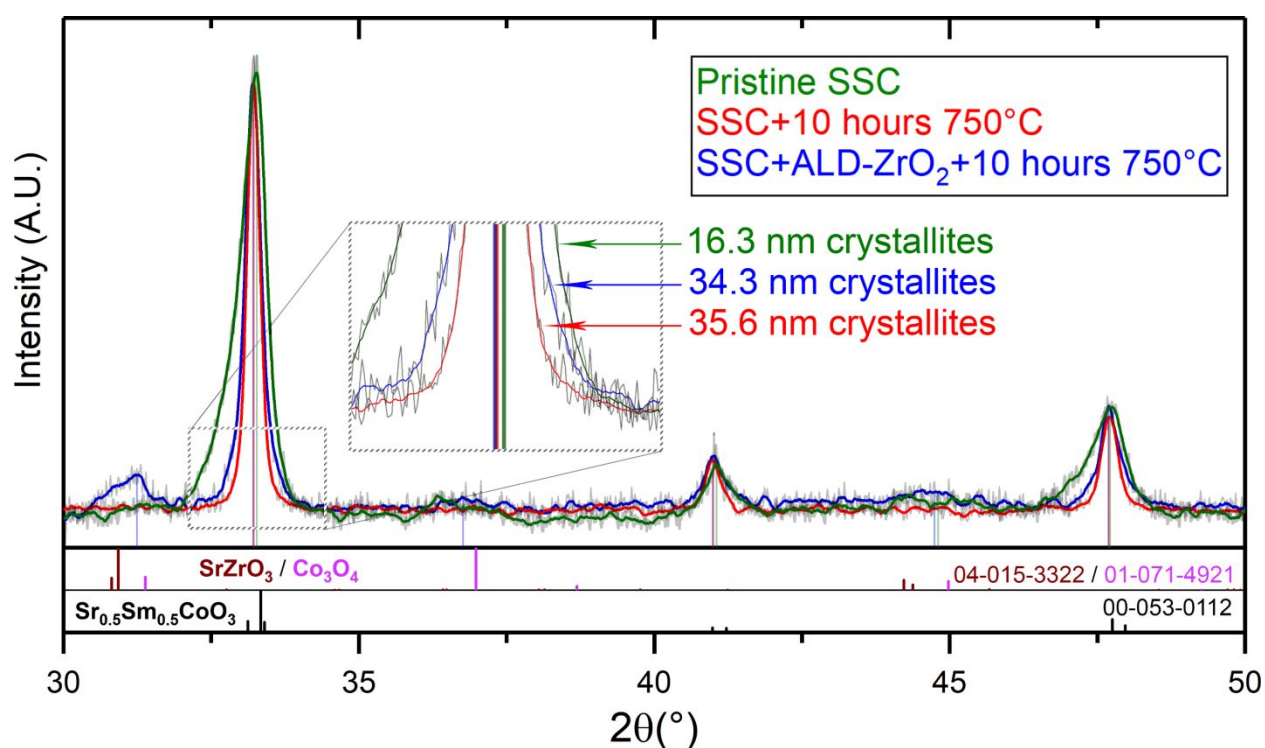


Fig. 7. XRD peak-shape comparison from broad (pristine sample) to narrow (annealed samples) with the sample having undergone ALD treatment narrowing less than the sample without, implying a smaller average crystallite size. PDF card numbers are included.

IV. Discussion

The polarization resistance of infiltrated SSC-GDC electrodes was observed to increase by ~30% over ~1000 h of accelerated testing at 750°C; similar degradation has been observed for other perovskite-based electrodes with infiltrated nano-scale structure, typically explained by particle coarsening or cation surface segregation.^{1,3,40} The present results show that ALD-ZrO₂ decreases the resistance degradation to 17-18% over 1000 h under these conditions. This result falls

between prior reports on the effect of ALD-ZrO₂ – in some cases degradation is almost eliminated,⁸ whereas in others there is no effect or even a negative effect.^{10,11} The present study utilizes chemical and morphological characterization of both the electrode and SSC powder to explore how ALD-ZrO₂ affects electrode characteristics. In the following, the implications of the results are discussed.

In order to understand the role of ALD-ZrO₂ on electrode performance, it is important to know the thickness of the ALD layer in the electrode active region, *i.e.*, within ~10 μm of the electrolyte.^{3,41,42} By scaling EDS Zr signal intensities measured versus position in the electrode (Fig. 4), the average ZrO₂ thickness in the active region was estimated to be 0.3 nm for the tested 30-cycle electrode, and 0.5 nm in the 60-cycle electrode. The substantial decrease in ZrO₂ thickness with increasing depth into the electrode can be attributed to the high aspect ratio of the porous structure, ~250 based on the pore diameter of ~100 nm and length of ~25 μm. The presence of the LSM current collector presumably also increases the effective aspect ratio. The comparatively more uniform Zr content in the un-infiltrated LSM layer may have occurred because of its higher porosity and larger pore size than the SSC-GDC functional layer. Given that the present ALD recipe was not designed to provide significant penetration, such a thickness gradient in the SSC-GDC is expected.^{43,44} For example, in a study of TiO₂ nanotubes with aspect ratios of ~180, a precursor exposure time of 0.5 s, comparable to our 0.4 s, led to a decrease in coating thickness down the length of a tube, dropping off by ~35% compared to an exposure times of >5 seconds.⁴³ However, a study of a ~250 aspect ratio Ni-YSZ electrode coated with a similar Zr precursor to the present case showed the deposition thickness quickly drop to 20% of the surface thickness at a depth of 25 μm, even with pulse times of 10 s; at depths > 30 μm, the ZrO₂ was not detected.⁴⁴

The active region ZrO₂ thickness is similar to the theoretical monolayer ZrO₂ thickness (0.327 nm thick).⁴⁵ Such thin ALD layers tend to show a discontinuous island structure, *e.g.*, that of the 3-cycle ALD coating in Fig. 3 (b), rather than layer growth.^{27,29} This may partially explain the good electrochemical performance of ALD-coated electrodes, *i.e.*, the coating did not substantially cover active sites on the SSC surface. The relatively low ZrO₂ layer thickness is also important because the present results show that ZrO₂ readily reacts with SSC, forming SrZrO₃ after 10 hours at 750°C (Fig. 6) and SmZrO₃ at 800°C. Given the present active-region ZrO₂ thicknesses of ~0.3 nm (30 cycles) or ~0.5 nm (60 cycles), only ~6% (or ~10% for 60 cycles) of the SSC would be reacted. Larger thicknesses would presumably consume and/or block a large enough fraction of the SSC to significantly degrade performance (*e.g.*, a thickness of 2.7 nm would be enough to entirely react all SSC present).

These results suggest the following interpretation of the life test data in Fig. 1. The initial decrease in R_p may result from the zirconate-forming reaction uncovering more active SSC sites. Once all ZrO₂ is reacted, the stable zirconate particles covering SSC surfaces may provide a barrier

to SSC coarsening, as suggested by the more stable R_p (Fig. 2) and reduced SSC particle coarsening (Fig. 7).

While SrZrO_3 is known to have a low conductivity and therefore is not expected to promote electrochemical activity, the other observed reaction products, SmCoO_3 and Co_3O_4 , may contribute to performance and stability; for example, there is evidence that infiltrated Co_3O_4 improves the initial polarization resistance in similar cathodes.^{13,46} It could also be suggested that the stability improvement results from ZrO_2 scavenging excess surface Sr on SSC; however, Sr segregation does not appear to be an important effect in SSC (Fig. 5).

Finally, note that the degradation rates quoted here are relatively large because the life tests were designed to accelerate degradation by using a temperature higher than that expected for cell operation, $\sim 600^\circ\text{C}$. In a prior study of the infiltrated SSC-GDC electrode system, accelerated test data was extrapolated to lower temperatures using a combined electrochemical and coarsening model, whereby 1000 h at 750°C corresponded to approximately 50,000 h at 600°C .³ The results suggest that the R_p of the present SSC-GDC electrodes with 50 nm SSC and Zr-overlayers would increase by $\sim 20\%$ over 50,000 h at a temperature of 600°C , relative to $\sim 30\%$ for the uncoated electrode. Thus the ALD induced stability improvement demonstrated here could provide a useful reduction in degradation.

V. Conclusions

The present results show that ALD- ZrO_2 improves the stability of infiltrated $\text{Sr}_{0.5}\text{Sm}_{0.5}\text{CoO}_{3-\delta}$ -GDC electrodes. The tentative explanation for the ALD effect is that coarsening of the nano-scale infiltrated SSC is suppressed. We propose that a non-continuous SrZrO_3 layer forms atop a network of nanostructured SSC shortly after initial heating of the ZrO_2 -coated electrode to operating temperature. Our results also indicate that the benefit of the SrZrO_3 was in the suppression of microstructural coarsening. Another likely degradation mechanism characteristic of this class of electrode, Sr segregation, was not found to be significant for SSC particles, given the lack of evolving Sr concentration detected in samples via ICP-OES.

The results suggest that the ALD- ZrO_2 thickness in the electrode's active region needs to be chosen correctly; if the ZrO_2 amount is too large, a significant portion of the SSC will be consumed in the reaction and/or the SSC surface may be mostly covered. Since the resulting SrZrO_3 phase has poor conductivity and electrochemical activity, electrode performance will be severely compromised. On the other hand, too thin of a layer would presumably lack sufficient ability to suppress coarsening. The present cases of 30- and 60-cycle ZrO_2 deposition, with average ZrO_2 thickness of ~ 0.3 nm and ~ 0.5 nm in the electrochemically active region, appears to be a reasonable amount because only ~ 6 - 10% of the SSC is consumed. Similar results are expected for other MIEC materials, most of which react with ZrO_2 .

The importance of ALD thickness and the difficulty of controlling and measuring the thickness may help explain the wide variations in reported results for ALD-ZrO₂ in MIEC electrodes. Obtaining the desired thickness is especially challenging because of the tendency for the ALD thickness to decrease with increasing depth into porous electrodes. In future work, a more uniform and well-controlled ZrO₂ thickness distribution with the TDMAZ precursor can presumably be achieved by increasing the exposure cycle time and lowering the reactor temperature, e.g., to 200°C.³⁰ It could also be helpful to reduce the thickness of the electrode and current collector, to the extent possible without compromising electrode performance.

VI. Conflicts of Interest

There are no conflicts of interest to declare.

VII. Acknowledgements

This work was mainly supported by the US Department of Energy Office of Science, award number DE-SC0016965 and the National Science Foundation, award OISE-1545907, that supported some of the microstructural characterization. Travis Schmauss was partially supported by a graduate fellowship provided by the Institute for Sustainability and Energy at Northwestern. The authors would also like to thank John Pieterse, Hongqian Wang, Kunli Yang, and Shanlin Zhang for experimental advice and assistance.

This work utilized Northwestern University Micro/Nano Fabrication Facility (NUFAB) and the Northwestern University Integrated Molecular Structure Education and Research Center (IMSERC), which are partially supported by Soft and Hybrid Nanotechnology Experimental (SHyNE) Resource (NSF ECCS-1542205), the Materials Research Science and Engineering Center (NSF DMR-1720139), the State of Illinois, and Northwestern University; the EPIC and Keck-II facilities of the NUANCE Center at Northwestern University, which has received support from the MRSEC program (NSF DMR-1121262) at the Materials Research Center, the International Institute of Nanotechnology (IIN), the Keck Foundation, and the State of Illinois, through the IIN; and the J.B.Cohen X-Ray Diffraction Facility supported by the MRSEC program of the National Science Foundation (DMR-1720139) at the Materials Research Center of Northwestern University and the Soft and Hybrid Nanotechnology Experimental (SHyNE) Resource (NSF ECCS-1542205.) Metal analysis was performed at the Northwestern University Quantitative Bio-element Imaging Center.

VIII. References

- 1 Z. Gao, L. V. Mogni, E. C. Miller, J. G. Railsback and S. A. Barnett, *Energy Environ. Sci.*,

- 2016, **9**, 1602–1644.
- 2 D. Ding, X. Li, S. Y. Lai, K. Gerdes and M. Liu, *Energy Environ. Sci.*, 2014, **7**, 552.
- 3 A. V. Call, J. G. Railsback, H. Wang and S. A. Barnett, *Phys. Chem. Chem. Phys.*, 2016, **18**, 13216–13222.
- 4 M. Shah, P. W. Voorhees and S. A. Barnett, *Solid State Ionics*, 2011, **187**, 64–67.
- 5 J. Fleig, *Annu. Rev. Mater. Res.*, 2003, **33**, 361–382.
- 6 J. Nielsen and J. Hjelm, *Electrochim. Acta*, 2014, **115**, 31–45.
- 7 J. H. Shim, G. D. Han, H. J. Choi, Y. Kim, S. Xu, J. An, Y. B. Kim, T. Graf, T. D. Schladt, T. M. Gür and F. B. Prinz, *Int. J. Precis. Eng. Manuf. Technol.*, 2019, **6**, 629–646.
- 8 Y. Gong, D. Palacio, X. Song, R. L. Patel, X. Liang, X. Zhao, J. B. Goodenough and K. Huang, *Nano Lett.*, 2013, **13**, 4340–4345.
- 9 Y. Gong, R. L. Patel, X. Liang, D. Palacio, X. Song, J. B. Goodenough and K. Huang, *Chem. Mater.*, 2013, **25**, 4224–4231.
- 10 M. Rahmanipour, Y. Cheng, T. M. Onn, A. Donazzi, J. M. Vohs and R. J. Gorte, *J. Electrochem. Soc.*, 2017, **164**, F879–F884.
- 11 R. J. Gorte, *DoE Technical Report: Cost-effective Manufacturing and Morphological Stabilization of Nanostructured Cathodes for Commercial SOFCs*, Washington, D.C., 2018.
- 12 H. J. Choi, K. Bae, D. Y. Jang, J. W. Kim and J. H. Shim, *J. Electrochem. Soc.*, 2015, **162**, F622–F626.
- 13 Y. Chen, A. Hinerman, L. Liang, K. Gerdes, S. P. Navia, J. Prucz and X. Song, *J. Power Sources*, 2018, **405**, 45–50.
- 14 R. Kungas, A. S. Yu, J. Levine, J. M. Vohs and R. J. Gorte, *J. Electrochem. Soc.*, 2012, **160**, F205–F211.
- 15 A. S. Yu, R. Kungas, J. M. Vohs and R. J. Gorte, *J. Electrochem. Soc.*, 2013, **160**, F1225–F1231.
- 16 H. J. Choi, K. Bae, S. Grieshammer, G. D. Han, S. W. Park, J. W. Kim, D. Y. Jang, J. Koo, J.-W. Son, M. Martin and J. H. Shim, *Adv. Energy Mater.*, 2018, **1802506**, 1802506.
- 17 C. Graves, 2012.
- 18 E. Jones, E. Oliphant and P. Peterson, 2001.
- 19 J. D. Hunter, *Comput. Sci. Eng.*, 2007, **9**, 99–104.
- 20 S. Van Der Walt, S. C. Colbert and G. Varoquaux, *Comput. Sci. Eng.*, 2011, **13**, 22–30.
- 21 M. Shah and S. A. Barnett, *Solid State Ionics*, 2008, **179**, 2059–2064.
- 22 J. G. Railsback, H. Wang, Q. Liu, M. Y. Lu and S. A. Barnett, *J. Electrochem. Soc.*, 2017, **164**, F3083–F3090.
- 23 T. Onn, R. Kungas, P. Fornasiero, K. Huang and R. Gorte, *Inorganics*, 2018, **6**, 34.
- 24 J. W. Elam, *At. Layer Depos. Nanostructured Mater.*, 2012, 227–249.
- 25 T. Keuter, N. H. Menzler, G. Mauer, F. Vondahlen, R. Vaßen and H. P. Buchkremer, *J. Vac. Sci. Technol. A Vacuum, Surfaces, Film.*, 2015, **33**, 01A104.
- 26 S. M. George, *Chem. Rev.*, 2010, **110**, 111–131.
- 27 R. L. Puurunen, W. Vandervorst, W. F. A. Besling, O. Richard, H. Bender, T. Conard, C. Zhao, A. Delabie, M. Caymax, S. De Gendt, M. Heyns, M. M. Viitanen, M. De Ridder, H. H. Brongersma, Y. Tamminga, T. Dao, T. De Win, M. Verheijen, M. Kaiser and M. Tuominen, *J. Appl. Phys.*, 2004, **96**, 4878–4889.
- 28 J. Liu, X. Meng, M. N. Banis, M. Cai, R. Li and X. Sun, *J. Phys. Chem. C*, 2012, **116**, 14656–

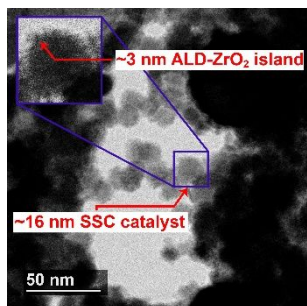
- 14664.
- 29 N. El-Atab, T. Gamze Ulusoy, A. Ghobadi, J. Suh, R. Islam, A. K. Okyay, K. Saraswat and A. Nayfeh, *Nanotechnology*, DOI:10.1088/1361-6528/aa87e5.
- 30 D. M. Hausmann, E. Kim and J. Becker, *Chem. ...*, 2002, 4350–4358.
- 31 H. Wang, K. J. Yakal-Kremiski, T. Yeh, G. M. Rupp, A. Limbeck, J. Fleig and S. A. Barnett, *J. Electrochem. Soc.*, 2016, **163**, F581–F585.
- 32 G. M. Rupp, A. Limbeck, M. Kubicek, A. Penn, M. Stöger-Pollach, G. Friedbacher and J. Fleig, *J. Mater. Chem. A*, 2014, **2**, 7099–7108.
- 33 G. D. Clayton and F. E. Clayton, *Patty's Industrial Hygiene and Toxicology. Volumes 2A, 2B, 2C, 2D, 2E, 2F: Toxicology*, John Wiley & Sons Inc., New York, NY, 4th edn.
- 34 L. Dieterle, D. Bach, R. Schneider, H. Störmer, D. Gerthsen, U. Guntow, E. Ivers-Tiffée, A. Weber, C. Peters and H. Yokokawa, *J. Mater. Sci.*, 2008, **43**, 3135–3143.
- 35 J. Matsuda, S. Kanae, T. Kawabata, J. T. Chou, Y. Inoue, S. Taniguchi and K. Sasaki, *ECS Trans.*, 2017, **78**, 993–1001.
- 36 S. Molin, W. Lewandowska-Iwaniak, B. Kusz, M. Gazda and P. Jasinski, *J. Electroceramics*, 2012, **28**, 80–87.
- 37 H. Sumi, T. Ohshiro, M. Nakayama, T. Suzuki and Y. Fujishiro, *Electrochim. Acta*, 2015, **184**, 403–409.
- 38 H. Tu and Y. Takeda, *Solid State Ionics*, 1997, **100**, 283–288.
- 39 U. Holzwarth and N. Gibson, *Nat. Nanotechnol.*, 2011, **6**, 534–534.
- 40 B. Koo, K. Kim, J. K. Kim, H. Kwon, J. W. Han and W. C. Jung, *Joule*, 2018, **2**, 1476–1499.
- 41 J. Fleig, *J. Power Sources*, 2002, **105**, 228–238.
- 42 C. Nicollet, A. Flura, V. Vibhu, A. Rougier, J. M. Bassat and J. C. Grenier, *Int. J. Hydrogen Energy*, 2016, **41**, 15538–15544.
- 43 R. Zazpe, M. Knaut, H. Sopha, L. Hromadko, M. Albert, J. Prikryl, V. Gärtnerová, J. W. Bartha and J. M. Macak, *Langmuir*, 2016, **32**, 10551–10558.
- 44 T. Keuter, G. Mauer, F. Vondahlen, R. Iskandar, N. H. Menzler and R. Vaßen, *Surf. Coatings Technol.*, 2016, **288**, 211–220.
- 45 D. M. Hausmann, E. Kim, J. Becker and R. G. Gordon, *Chem. Mater.*, 2002, **14**, 4350–4358.
- 46 H. Zhang, H. Liu, Y. Cong and W. Yang, *J. Power Sources*, 2008, **185**, 129–135.

ZrO₂ Atomic Layer Deposition Into Sr_{0.5}Sm_{0.5}CoO_{3-δ}-Ce_{0.9}Gd_{0.1}O₂₋₆ Solid Oxide Fuel Cell Cathodes: Mechanisms of Stability Enhancement

Travis A. Schmauss^a, Justin G. Railsback^a, Matthew Y. Lu^a, Kevin Y. Zhao^a, Scott A. Barnett^{a*}

^aDepartment of Materials Science and Engineering, Northwestern University, Evanston, IL 60208. E-mail: s-barnett@northwestern.edu

Table of Contents Entry



Atomic layer deposition of ZrO₂ creates reactive islands that limit coarsening and improve the stability of fuel cell cathode Sr_{0.5}Sm_{0.5}CoO_{3-δ}-Ce_{0.9}Gd_{0.1}O₂₋₆.

20 words.